LANGMUIR Article
Cite This: Langmuir 2018, 34, 1410−1418
pubs.acs.org/Langmuir

Blooming of Smectic Surfactant/Plasticizer Layers on Spin-Cast Poly(vinyl alcohol) Films

Arron Briddick,[†] Rebecca J. Fong,[†] Elise F. D. Sabattié,[†] Peixun Li,[‡] Maximilian W. A. Skoda,[‡] Florence Courchay,[§] and Richard L. Thompson*[,†]

[†]Department of Chemistry, Durham University, Science Site, Durham DH1 3LE, U.K.
[‡]STFC ISIS Facility, Rutherford Appleton Laboratories, Chilton, Didcot OX110QX, U.K.
[§]Procter&Gamble, Brussels Innovation Center (BIC), Temselaan 100, 1853 Strombeek Bever, Brussels, Belgium

Supporting Information

ABSTRACT: The blooming of sodium dodecyl sulfate (SDS) and the influence of plasticizer (glycerol) on the surfactant distribution in poly(vinyl alcohol) (PVA) films have been explored by neutron reflectometry (NR) and ion beam analysis techniques. When in binary films with PVA, deuterated SDS (d_{25}-SDS) forms a surface excess corresponding to a wetting layer of the surfactant molecules at the film surface. The magnitude of this surface excess increased significantly in the presence of the plasticizer, and the surfactant was largely excluded from the PVA subphase. NR revealed smectic nanostructures for both SDS and glycerol components within this surface excess in plasticized films. This combined layer comprises surfactant lamellae, separated by interstitial glycerol-rich layers, which is only formed in the plasticized films and persists throughout the surface excess. Atomic force microscopy micrographs of the film surfaces revealed platelike structures in the plasticized PVA, which were consistent with the rigid defects in the surfactant-rich lamellae. The formation of these structures arises from the synergistic surface segregation of SDS and glycerol, evidenced by surface tensiometry. Cloud point analysis of bulk samples indicates a transition at ∼55% water content, below which phase separation occurs in ternary films. This transition is likely to be necessary to form the thick wetting layer observed and therefore indicates that film components remain mobile beyond this point in the drying process.

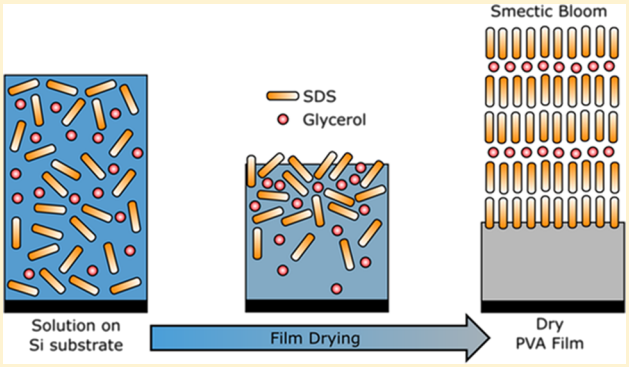

INTRODUCTION

Poly(vinyl alcohol) (PVA) is a semicrystalline synthetic polymer that has been widely exploited for its ability to form high-quality optically transparent films. Characteristics such as degree of hydrolysis (DH) and degree of polymerization must be carefully controlled to provide optimal physical properties such as strength and solubility of PVA films.[1,2] For many industrial applications, pure PVA films are too brittle and inflexible; hence, plasticizers are introduced into the system. Glycerol has been shown to be a compatible plasticizer[3] and is utilized in many cases to improve film flexibility while retaining good levels of tensile and shear strength.

The prediction of surfactant behavior in polymer films and the tendencies of small molecules to migrate and segregate remains a fundamental scientific challenge, which has received relatively little attention compared to the solution properties of these materials. However, segregation of surfactants has been shown to be very important in the formation and physical properties of latexes.[4,5] Our inspiration to study the surfactant behavior in these films derives from the number of applications in which plasticized PVA films encounter surfactant-rich environments. PVA is increasingly used to encapsulate surfactant-rich formulations for soluble unit dose laundry and dishwashing applications. The presence and migration of surfactants have potential to interfere with processes such as aging in polymer films, which, in turn, may have a profound impact on product performance and lifetime.

Previously, we reported the surface segregation behavior of cationic and nonionic surfactants in plasticized PVA films and observed that whereas glycerol suppressed the surface activity of the nonionic surfactant in PVA, the opposite trend was seen for the cationic surfactant.[6] It appears that surface segregation is brought on by both surface energy differences and incompatibility between surfactant, plasticizer, and polymer. The initial driver for surface segregation is the difference in surface energy, favoring surface segregation of the lowest surface energy component. Incompatibility between the components can significantly increase the surface segregation and even the

Received: November 27, 2017
Revised: December 22, 2017
Published: January 2, 2018

DOI: 10.1021/acs.langmuir.7b04046
Langmuir 2018, 34, 1410−1418

formation of a wetting layer, but the molecular origins of this behavior are challenging to establish in multicomponent systems including amphiphilic materials.

To build a more complete picture of surfactant segregation in PVA, we therefore focus here on the behavior of the anionic surfactant sodium dodecyl sulfate (SDS). This system is particularly relevant to detergent applications of PVA because anionic surfactants are commonly included in these formulations. Ion beam analysis (IBA) has been used to establish the surface and interfacial segregation behavior of this surfactant in thin PVA films cast onto a silicon substrate. We have used neutron reflectometry (NR) with deuterium labeling to resolve the interface between the segregated layers and the PVA film, which can give some insight into the compatibility and interactions, and finally atomic force microscopy (AFM) has been employed to study the lateral structuring and, for the first time, tackiness of the film surface via adhesion measurements.

EXPERIMENTAL SECTION

Materials and Sample Preparation. PVA resin (Sigma-Aldrich P8136, M_w = 30−70 kg/mol, DH = 87−90%), glycerol (Aldrich), d_5-glycerol (CK isotopes), and hydrogenous SDS (h-SDS, Aldrich) were purchased and used as received. Deuterated SDS (d_{25}-SDS) was synthesized at the Rutherford Appleton Laboratories according to the method described elsewhere.[7]

PVA was dissolved in deionized water by heating to 75 °C with stirring to create 4 w/v % solutions. Similar aqueous solutions of other components (glycerol, d_5-glycerol, h-SDS, and d_{25}-SDS) were also made at 4% (w/v). Final 4% (w/w) solutions containing the desired proportion of the polymer with surfactant and/or glycerol were prepared by mixing the relevant solutions for >3 h. These solutions were then spin-cast to form films of between 120 and 250 nm thickness. The solutions were spun on to fresh silicon wafers that had been cleaned with acetone prior to use to remove all traces of hydrophobic impurities, ensuring consistent film production. The evaporation stage of spin coating, during which rapid changes in film color are apparent because of the optical interference, is complete within approximately 30 s, regardless of the film composition and plasticizer content. Films were prepared in the same way for NR except that the substrates were 55 mm diameter and 5 mm thick silicon blocks.

Ion Beam Analysis. The application of IBA techniques including Rutherford backscattering spectroscopy (RBS) and nuclear reaction analysis (NRA) to soft matter have been described in our previous work and can also be found in greater detail elsewhere.[8−10] As IBA operates under vacuum conditions (<4 × 10^{-6} Torr), loss of low-molecular-weight components from polymer films can occur; hence, liquid-nitrogen sample cooling to below −50 °C was required to vitrify the samples before analysis. This process maintains the water content of the films during analysis under vacuum.[11] RBS measurements were made with a 1.5 MeV $^4He^+$ incident ion beam at 65° to the sample normal. A Canberra PIPS detector with a nominal energy resolution of 17 keV was used to detect the energy of backscattered $^4He^+$ ions at 170° to the incident beam in Cornell geometry. A depth resolution of ∼15 nm is achievable with RBS under these experimental conditions. NRA measurements were taken with the same detector setup except for 700 keV, $^3He^+$ ion beam, and a grazing angle of incidence of 80° to the sample normal were used.

Whereas RBS relies on differences in elemental mass to identify the depth distribution of components in films, NRA achieves this for materials lacking such contrast via deuterium labeling. Deuterium-labeled glycerol and surfactants have been used to isolate the depth distribution of individual components in complex mixtures. When performing NRA under the experimental conditions described, a depth resolution of ∼8 nm can be achieved. Although this depth resolution is insufficient to describe any orientational features of the surfactants in thin layers, it is sufficient to quantify surfactant segregation; hence, quantification of surface enrichment is possible, even if films are too rough or crystalline to address with NR.

For all IBA experiments, DataFurnace software (Surrey University, WiNDF v9.3.68 running NDF v9.6a)[12] was used to compute concentration versus depth profiles. To generate depth profiles in units of length as opposed to atoms/cm^2, densities of all molecules in the sample were required (PVA, glycerol, and SDS at 1.19, 1.26, and 1.01 g cm^{-3}, respectively, were used). DataFurnace uses a multilayer description of films. The composition and thickness of each layer were allowed to vary, and the calculated ion beam spectra from the simulated structures were iteratively fitted to the experimental data. To restrict the number of variables, model composition profiles were permitted to have a maximum of three layers.[13−15]

Neutron Reflectometry. NR is well-established as a key technique for studying structural organization of soft matter including surfactants and polymers in solution.[16] A significant advantage of this technique over most other surface characterization methods of comparable resolution is its ability to work at atmospheric pressure, which enables the study of samples under shear[17] or controlled atmosphere.[18] The SURF and INTER reflectometers at the Rutherford Appleton Laboratories were utilized to obtain vertical concentration versus depth profiles. Samples were prepared in a way similar to that used for IBA except for they were made thinner (∼70 nm) by increasing the rotational speed of the drying stage when spin-coating. NR was used to provide both better depth resolution (∼0.5 nm) and analysis under atmospheric conditions. Here, the same deuterium labeling that was used in NRA also provided contrast between the components for NR via the difference in scattering length density (SLD) of these components. The SLDs of the materials used are presented in Table 1. A complete reflectivity curve (from the critical edge to the background) was obtained by measuring three incident angles, resulting in a momentum transfer (Q) range of 0.008 < Q/Å^{-1} < 0.35. NR experiments over this Q range required a significant acquisition time (∼2 h per sample). Any change in sample thickness or composition over this period would eradicate the Kiessig fringes from which the sample thickness is determined. Therefore, samples must be stable for a minimum of 2 h for the acquisition to be successful.

Table 1. List of Scattering Length Densities for Hydrogenous and Deuterated Materials

component	SLD/10^{-6} Å^{-2}
PVA	0.72
Si	2.07
glycerol	0.61
d_5-glycerol	4.91
h-SDS	0.34
d_{25}-SDS	5.83

Atomic Force Microscopy. The surface properties of the spin-cast polymer films were analyzed using a Bruker Multimode 8 scanning probe microscope. Equipped with an E-type scanner, AFM is capable of scanning grids of 15 × 15 μm^2. Quantitative nanomechanical analysis mode was used to analyze the films. Once a 1 μm × 1 μm scan was obtained, the image was "flattened" using NanoScope Analysis (v 1.1.) to remove the natural curvature of height caused as the sample is rastered relative to the cantilever.

Surface Tensiometry. The surface tensions of dilute aqueous solutions of PVA, glycerol, and SDS were measured using a KRÜSS K10 tensiometer, equipped with a Du Nouy ring. The platinum ring was cleaned by holding it in a flame. Solutions were prepared using ultrahigh purity water, and surface tension measurements were performed at 20 °C. Repeat measurements were taken to check the reproducibility, and the accuracy of the measurements taken was 0.1 mN/m.

Cloud Point Measurements. Dilute solutions (∼0.4 g) were prepared at defined ratios of PVA and SDS, in which the initial solute concentration was typically 10% (w/w). These solutions were applied to a glass slide, which was thermostatted to 40 °C. The mass of the

DOI: 10.1021/acs.langmuir.7b04046
Langmuir 2018, 34, 1410−1418

solution was regularly monitored, and the point at which the solution became cloudy was determined by visual inspection.

RESULTS

Segregation of Individual Components in PVA Films. The results are presented as composition versus depth profiles for individual components within PVA films. The derived numerical parameters (layer thickness, concentration, SLD, and roughness) for the displayed concentration profiles are tabulated in the Supporting Information (S.I.1.). Using NR and IBA, we have previously established that glycerol exhibits a homogeneous vertical composition profile in PVA,[6] which is consistent with previous reports indicating its low surface activity.[3]

The surface segregation of SDS was studied using a deuterated analogue of the surfactant, d_{25}-SDS. The deuterium labeling enabled the measurement of high-precision depth profiles by NR and NRA. Figure 1a shows the NRA data for 10 and 20% d_{25}-SDS in PVA, and as can be seen, a surface excess of surfactant is evident in both data sets. Additional characterization using RBS to identify the approximate depth distributions from the S and Na atoms yielded consistent results, which are included as Supporting Information (S.I.2 and S.I.3).

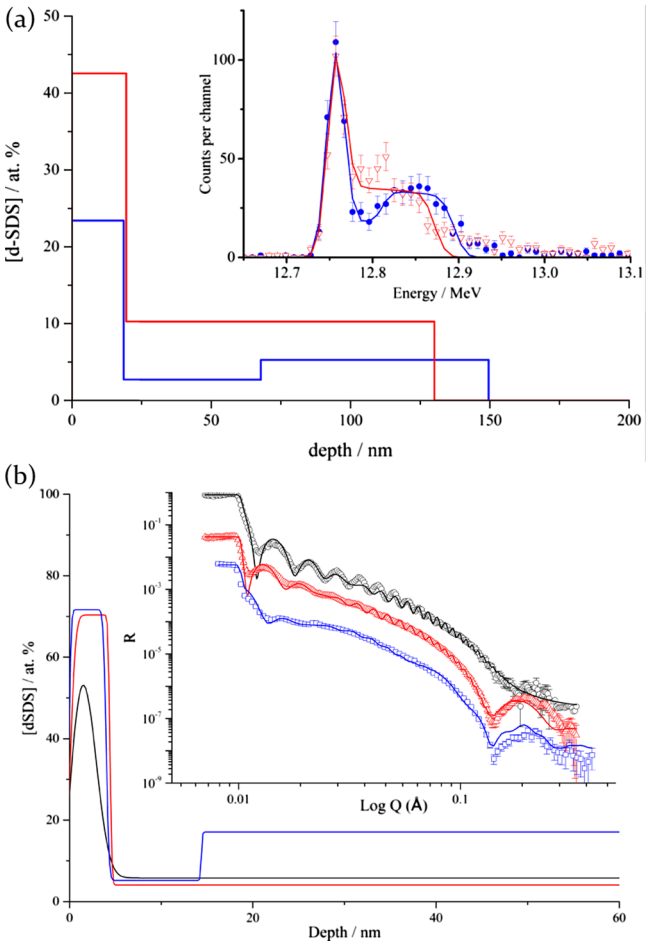

Figure 1. (a) NRA data and fits (inset) for 10% (blue, circles) and 20% (red, triangles) d_{25}-SDS in thin PVA films. (b) NR data (offset) and fits for 5% (black, open circles), 10% (red, open triangles), and 20% (blue, open squares) d_{25}-SDS in thin PVA films. The derived concentration profiles of d_{25}-SDS correspond to the fitted curves.

The surface excess is defined as

$$z^* = \int_0^\infty \varphi(z) - \varphi_b \, dz \quad (1)$$

where φ_b is the bulk concentration adjacent to the surface excess region and $\varphi(z)$ is the depth (z)-dependent volume fraction profile of the near-surface region. As the average concentration of d_{25}-SDS in the film is increased from 10 to 20% (w/w %), the surface excess increases from 3.8 to 6.6 nm and the bulk concentration also rises. A depleted region of the surfactant is evident below the surface excess for the 10% d_{25}-SDS data in Figure 1a, which is clearly identifiable from the minimum in the raw data at ∼12.8 MeV. This feature suggests either phase separation of the components within the film or a state of incomplete equilibration.

Figure 1b shows the NR data, fits, and the corresponding surface enrichment of SDS for 5, 10, and 20% d_{25}-SDS in PVA. The presence of a surface excess of surfactant is confirmed by the NR data. A layer of ∼4 nm 50% d_{25}-SDS is formed at the surface when 5% surfactant is present, and the concentration and thickness of this excess appear to reach a limiting value at higher surfactant concentrations. With increasing d_{25}-SDS concentration in pure PVA, the surface excess appears to be quite constant (∼4.5 nm) and the bulk concentration steadily rises. This mode of behavior is qualitatively consistent with a surfactant above the critical micelle concentration (cmc), where increasing the concentration has almost no effect on the activity and therefore does not influence the surface concentration. The small discrepancy between z^* measured by NR and that measured by NRA is attributable to the lower film thickness of the NR sample. In this limit of very thin films, z^* is often limited by the amount of surfactant available, and in a two-phase mixture, the thickness of a wetting layer at equilibrium would be expected to depend directly on the film thickness. Although a detailed study of film thickness effects is beyond the scope of this work, we note that the ratio of the surface excess (NRA/NR) 6.6/4.5 is approximately consistent with the ratio of the film thickness 130/99.

Influence of Glycerol Plasticizer on d_{25}-SDS Ionic Surfactant. Although in binary films with PVA, glycerol showed no evidence of surface segregation,[6] when added to films containing SDS and PVA, it appears to have a profound impact on the depth distribution of the surfactant. Figure 2 shows the influence of (hydrogenous) glycerol concentration on the depth distribution of 20% d_{25}-SDS in PVA. When glycerol is included in the film, the surface excess of d_{25}-SDS is greatly increased. This is evident as a large increase in both thickness and mass fraction of d_{25}-SDS in the initial 30 nm of the film, which is offset by a decrease in the "bulk concentration" of d_{25}-SDS below the surface. The same phenomenon was observed with NR, as shown in the depth profiles in Figure 3. The amount of surfactant present at the surface shows a large increase upon plasticization with glycerol, with a corresponding reduction in the bulk surfactant concentration.

Initial fitting of the NR data using a model that included the surface excess as a continuous feature as suggested by NRA is shown in the Supporting Information (S.I.4). Although these fits captured $R(Q)$ very well for $Q < 0.1$ Å^{-1} and were consistent with the output of the NRA experiments, they failed to reproduce the significant feature (a weak Bragg peak) in $R(Q)$ for $Q \approx 0.15$ Å^{-1}. This would suggest that some repeating structures on a scale of $\sim 2\pi/Q_{peak}$ (∼4 nm) are missed by this

DOI: 10.1021/acs.langmuir.7b04046
Langmuir 2018, 34, 1410−1418

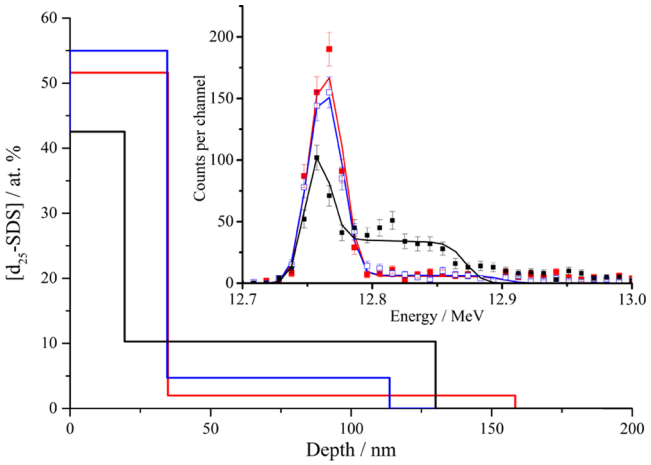

Figure 2. NRA data, fits, and composition profiles for 20% d_{25}-SDS (black, filled squares), 20% d_{25}-SDS and 10% h-glycerol (red, filled squares), and 20% d_{25}-SDS and 20% h-glycerol (blue, open squares) in thin PVA films.

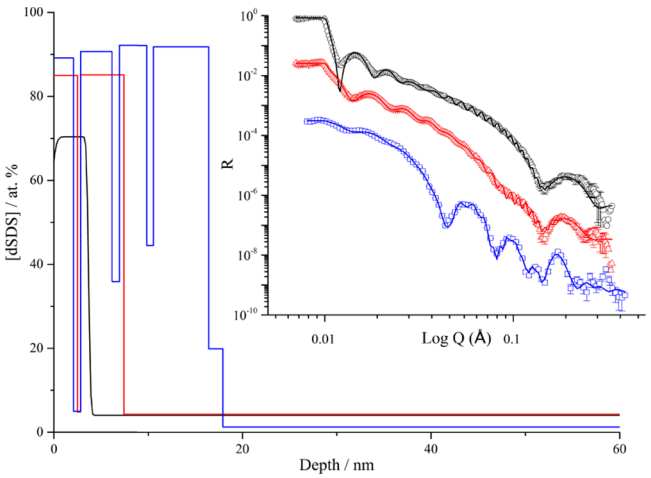

Figure 3. NR data (offset), fits, and composition profiles for 5% d_{25}-SDS and 20% glycerol (black, open circles), 10% d_{25}-SDS and 20% glycerol (red, open triangles), and 20% d_{25}-SDS and 20% glycerol (blue, open squares) in thin PVA films.

simple single-layer model.[19−21] By including a more complex structure that allows for some internal structure of the SDS layer, much more precise fits to the NR data are achievable across the entire measured Q range (Figure 3, inset). Here, we have still restricted the model to symmetric interfaces between layers to avoid overparameterization. Significantly, this model structure is also consistent with the IBA results for similar systems, which would not have been able to resolve such fine structures. For clarity, the roughness between discrete layers has been removed from the composition profiles displayed in Figure 3. Some contribution to the measured roughness would be expected, even for perfectly aligned d_{25}-SDS multilayers, because of the variation in SLDs between the head and tail groups of the surfactant molecules. An example of a depth profile before and after roughness removal can be found in the Supporting Information (S.1.5.), where the distinct layers of the surfactant are less obvious prior to the roughness removal.

At lower concentrations of the surfactant (∼5%), the plasticized PVA films exhibit single-layer surface segregation of the surfactant compared to the nonplasticized films. It is only at higher concentrations of surfactant (≥10%) where these additional multilayer features develop. The average concentrations of the fitted compositions are consistent with those of the solution compositions of the spin-cast films. The formation of a large surface excess at higher average compositions coincides with the bulk composition in the film being lower than the average composition. Figure 3 indicates the highly concentrated regions of the surfactant, separated by regions of depleted surfactant within the surface excess. From the concentration (∼90 at. %) and the thickness (2.9−3.3 nm) of these surfactant layers, it appears that SDS at the surface of these films forms a smectic assembly of bilayers. Coiro et al.[22] state the thickness of SDS lamellae to be ∼4 nm in highly concentrated aqueous solutions, which were separated by a "polar slab". This situation is similar to what we find by NR for the thickness and nature of segregated layers on PVA. The depleted regions of the surfactant which separate the surfactant bilayers are caused by a relatively low SLD of the compounds (PVA or glycerol) present at that specific depth within the film.

By altering the deuterium-labeling regime such that the glycerol was deuterated instead of the SDS, NR could isolate the concentration profile of glycerol in the presence of SDS and PVA. Analysis of the 20% h-SDS and 20% d_5-glycerol sample (Figure 4) revealed that the regions between the layers of pure SDS shown in Figure 3 are in fact enriched with the d_5-glycerol plasticizer. Figure 4 depicts the NR data for the sample and four simulations, in which the number of layers is systematically varied. It can easily be seen from the trial depth profiles that the best model, which replicates the intensity of the Bragg peak, is achieved when four glycerol-rich layers are included.

Surface Properties of Plasticized PVA with SDS. Figure 5 displays the height and adhesion maps obtained by AFM of the PVA film containing 20% h-SDS, with or without the presence of glycerol. Control experiments for the same film without SDS appeared rather featureless, similar to the SDS in PVA without glycerol, and are included as Supporting Information (S.I.6). All films are smooth on the scale of a few nanometers and hence are suitable for analysis by NR. Root-mean-square (R_q) roughness values for all AFM samples are displayed in Table 2. Although AFM appears to resolve slightly different features in every film, it should be noted that the variation in height in all but the PVA + SDS + glycerol film is only marginally greater that the vertical resolution (∼0.3 nm). In these measurements, the units of the adhesion scale are arbitrary, but because the same probes were used in each case, the scale is consistent between samples.

The PVA film incorporating both SDS and glycerol is qualitatively distinct from either the pure PVA film or the PVA films which incorporate a single additional component. Including the plasticizer and surfactant simultaneously leads to the development of some "platelike" structures on the sample surface that are on the order of 1 nm higher than the surrounding material with a lateral dimension of 100−500 nm. Furthermore, the adhesion map reveals patches of reduced adhesion at the edges of the plates, which were not seen in any of the control samples, and echoes the pattern of the platelike structures. These features are consistent with the formation of a solid layer of self-assembled SDS, which is slightly less tacky than the plasticized PVA. Overall, the AFM results appear to support evidence of significant restructuring of PVA films when both SDS and glycerol are simultaneously present.

Surface Activity in Dilute Solutions. Surface tensiometry was used to characterize the surface activity of individual

DOI: 10.1021/acs.langmuir.7b04046
Langmuir 2018, 34, 1410−1418

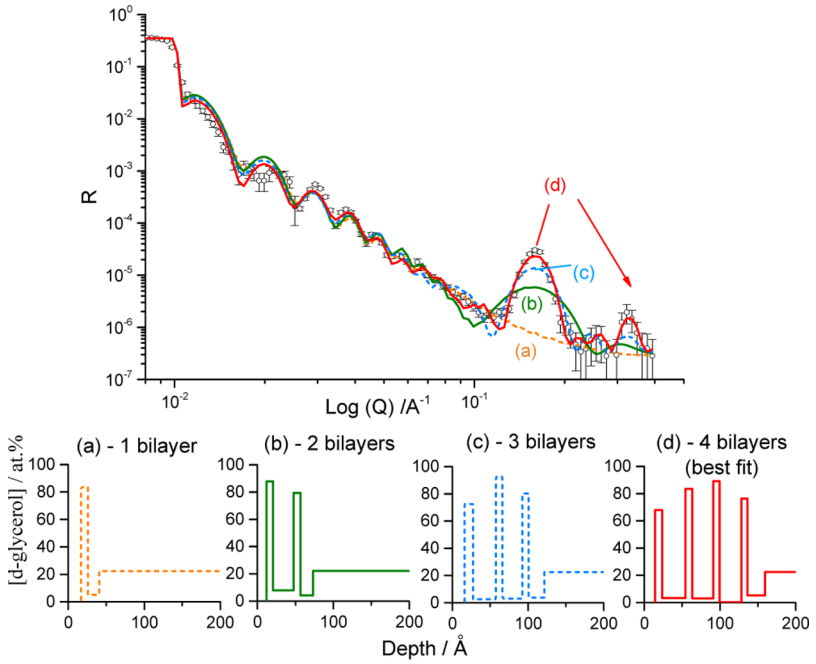

Figure 4. NR data, fit, and depth profile for 20% h-SDS and 20% d_5-glycerol in a thin PVA film and four trial fits for increasing layers of glycerol at the surface of the film.

components in dilute solutions. The results presented in Figure 6 show that at very low solute levels, PVA gives rise to the greatest reduction in surface tension. Although less active at very low concentrations, SDS surface tension drops sharply toward a cmc of ∼0.14% (w/w).[23] We note (as has been well-established elsewhere[24]) a small minimum in surface tension close to the cmc, which arises from trace quantities of dodecanol which are present as a hydrolysis product of SDS. At higher concentrations, SDS reaches a significantly lower minimum surface tension than either of the other solutes, and this is the most relevant region of surface activity for films that would be prepared from relatively concentrated mixtures. Although glycerol does give rise to some reduction in surface tension, this highly polar molecule is the least surface-active component other than water.

Despite the negligible surface activity of glycerol in pure water (Figure 6), it has a significant influence on the surface activity of SDS. Figure 7 shows the concentration dependence of SDS on surface tension in solutions, in which a defined quantity of glycerol is also present in the water. At low surfactant concentrations, the presence of glycerol behaves synergistically and enhances the efficiency of the surfactant, giving rise to a greater reduction in surface tension than that for the pure aqueous system. The cmc is also very slightly reduced, which may account for the loss of the minimum in surface tension attributed to dodecanol.

Analysis of the miscibility of components is shown as a ternary phase diagram for water, SDS, and PVA in Figure 8. In the context of the present work, phase transitions associated with the drying of solution-cast films are of particular interest. The arrow indicates the direction of the changing composition for a drying film of 20% SDS corresponding to the composition profile shown in Figure 1. As the water content drops below 55% (w/w), the film becomes cloudy, suggesting that the components are no longer stable as a single phase. For quite a broad range of SDS/PVA, the phase boundary occurs at a similar stage in the drying process. The notable exception to this is for pure PVA and water, which, in the absence of SDS, appears to be miscible in all proportions.

DISCUSSION

Surface Enrichment in Two-Component PVA Films. Whereas glycerol was found to be homogenously distributed, the surfactant SDS shows a distinct surface activity in PVA films, which may be rationalized through surface energy values. Various sources in the literature report the solid surface energy of PVA, similar to that used in this work, to be ∼40 mN/m.[6,25−29] In comparison, glycerol surface tension was measured to be 63.8 mN/m at 20 °C, which is in agreement with the literature values.[30] Thus, glycerol would not be expected to adsorb to the surface of PVA. Much work has been done on the calculation of surface tension for SDS, both in its pure form and in aqueous solution. Mysels quotes the values from several authors, with pure SDS surface tension values ranging from 48.4 to 52.5 mN/m.[24] These values are generally higher than those established for PVA, so spontaneous surface segregation might not be expected on the basis of this comparison. However, for our purposes and indeed for most industrially produced PVA films, the relative surface activity in each component in water is more relevant because films are produced from a mixed aqueous solution. Our surface tensiometry results of PVA solutions reveal a trend similar to that of the early work of Frisch and Al-Madfai, which was carried out on a near-identical DH of PVA.[31] This paper also reported that the approach to equilibrium was slow for PVA solutions and the surface tension approached the equilibrium value at a rate that could be described by an exponential decay with a characteristic relaxation time on the order of an hour.

The limiting surface tensions of PVA and SDS, together with the relatively slow adsorption of PVA in dilute solutions, provide some useful insights into the behavior that we observe for our spin-cast films. Even after allowing for the PVA concentration in our films to exceed the surfactant concentration by a factor of 4−20, the PVA is relatively inactive at

DOI: 10.1021/acs.langmuir.7b04046
Langmuir 2018, 34, 1410−1418

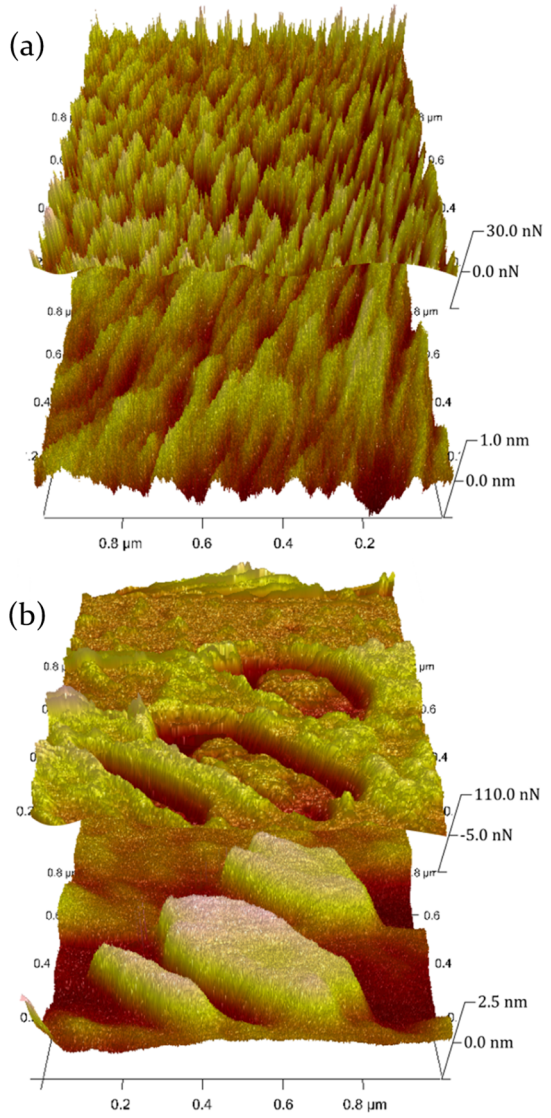

Figure 5. (a) AFM height map and overlaid adhesion plot for a 20% h-SDS spin-cast thin film. (b) AFM height map and adhesion plot for a 20% h-SDS and 20% h-glycerol PVA thin film.

Table 2. Influences of Glycerol and SDS on the Root-Mean-Square Roughness Values of Spin-Cast PVA Films

film	R_q/nm
PVA	0.190
PVA + glycerol	0.249
PVA + SDS	0.205
PVA + SDS + glycerol	1.140

aqueous solution surfaces, and indeed the slow kinetics of PVA adsorption may also tend to result in the aqueous film surface being seeded with SDS. At the initial solution concentrations for spin casting, 3−4% (w/v) PVA and 0.25−1% SDS, Figure 6 reveals that SDS has a significantly greater surface activity. When the faster adsorption of the low-molecular-weight surfactant is also taken into account, the surface excess of SDS in the final film is then a logical consequence of the drying process.

It appears that the surface enrichment of SDS while water is present may act as a template for the adsorption of further SDS as the film dries and the components become immiscible. The

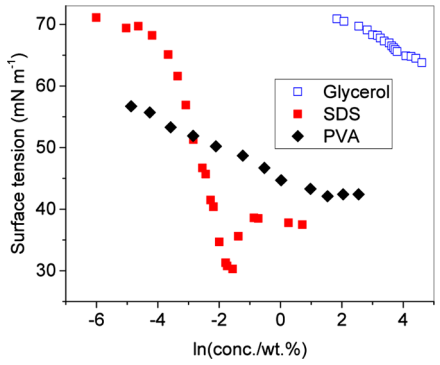

Figure 6. Concentration dependence of surface tension for SDS, glycerol, and PVA in aqueous solutions.

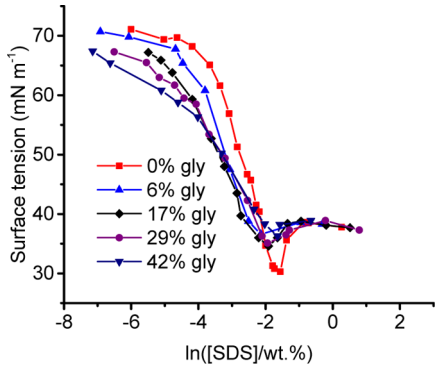

Figure 7. Influence of glycerol concentration (indicated in the legend) on the surface tension of aqueous SDS solutions.

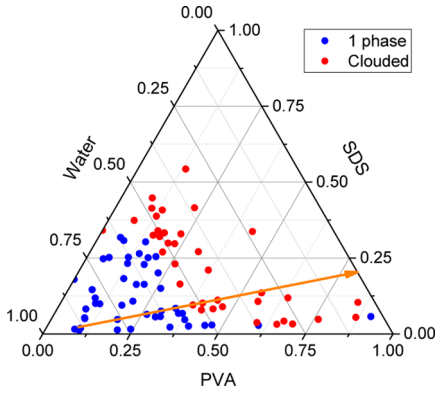

Figure 8. Cloud point analysis of ternary water/SDS/PVA mixtures at 40 °C. The arrow indicates the composition variation for a drying process in which the PVA/SDS ratio is fixed at 80:20.

surface excess values for SDS in the unplasticized PVA films (Figure 1) appear to correspond to a wetting layer of the surfactant. (The average length of an SDS molecule has been calculated to be 1.36 ± 0.07 nm;[32] therefore, the measured z^* value is much thicker than that could be accounted for by a monolayer of the surfactant at the surface.) Because a complete wetting layer of the surfactant on the PVA film would not be expected in a single-phase mixture, it appears that the film components remain mobile in the drying film until some point beyond the cloud point at 55 w/w % water.

Influence of Plasticizer on the Structure of the Surface Excess. Although NRA lacks the resolution required to characterize the self-organization of the d_{25}-SDS chains, it unambiguously reveals the presence of adsorption at the surface

DOI: 10.1021/acs.langmuir.7b04046
Langmuir 2018, 34, 1410−1418

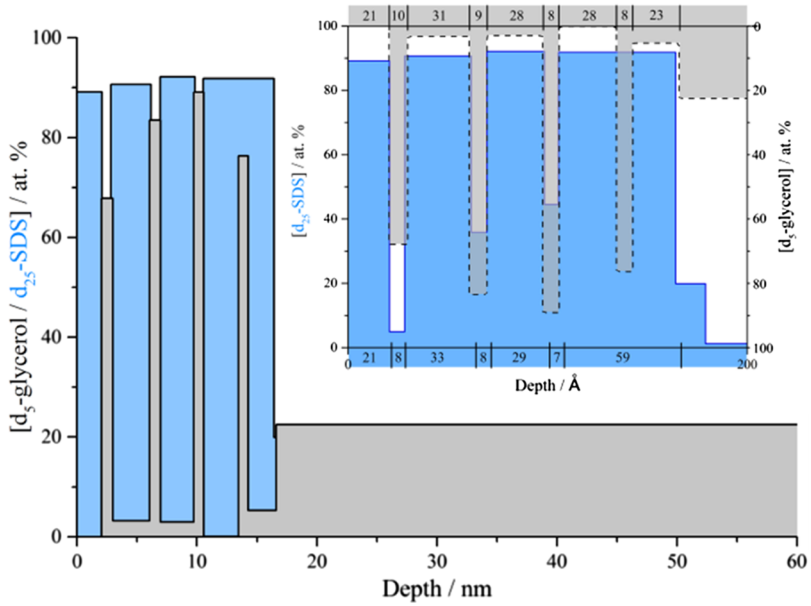

Figure 9. Combined plot of the composition profiles in which d-labeling has been used to isolate glycerol or SDS in turn. The inset highlights the composition profiles of surface excesses (inset) and h-SDS profile inverted (gray) with layer thickness values displayed for each profile outside of the axis, displaying the degree to which the plots agree.

in multilayer quantities, suggesting the presence of a wetting layer of the surfactant. These results underpin the high-precision analysis by NR, which resolves the presence of multiple smectic SDS and glycerol layers, spontaneously bloomed on the surface of spin-cast PVA films. We have not previously seen layered structures for nonionic surfactants, although in these systems, the total surface excesses were smaller, and thus any such layering would be less apparent.[6] It is also likely that the surfactant structures have different packing parameters in the glycerol/PVA environment. It appears that the layering of d_{25}-SDS persists throughout the surface excess. If the packing parameter favored another structure with a different curvature, then the lamellar ordering would be expected to decrease further from the surface.

Figure 9 shows the concentration profiles for both the 20% d_{25}-SDS and 20% d_5-glycerol samples overlaid as well as the plot of the surface excess region in the inset, with the depth profile for the 20% d_5-glycerol sample inverted. It can be seen that when inverted, although the d_{25}-SDS/h-glycerol and h-SDS/d_5-glycerol profiles are obtained from separate samples, they interlock remarkably well, suggesting that glycerol and SDS form part of one coadsorbed structure on the PVA surface. The only discrepancy between the two plots is that there appears to be an additional layer captured in the d_5-glycerol sample, which was not apparent in the d_{25}-SDS fit. This small discrepancy probably reflects the fact that two slightly different films are being compared, in which the compositions are very closely, but not perfectly, matched. Within this limitation, the combined data provide strong evidence for the existence of a multilayered glycerol−SDS structure at the surface of the film.

Complex surfactant multilayers, albeit in the bulk of an aqueous medium, have been previously documented.[22,33] Coiro et al. reported a series of stacked ∼4 nm surfactant lamellae that were found to be separated by polar slabs in highly concentrated aqueous solutions.[22] Despite the systems studied here being polymer-based, a remarkably similar lamellae thickness and polar slab presence are observed from the NR fits. Previously, ability of these multilamellae to form in the bulk was believed to be facilitated by the presence of water in the middle of the polar slab, which is the region defined by the surfactant headgroups. Incorporation of water encourages lamellae development by screening the ion−ion interactions of the surfactant headgroups and forms hydrogen bonds between the sulfate groups of opposing monolayers. In our experiments, it appears that the addition of glycerol plays a similar role in enabling lamellar structures to develop on the film surface. Figure 10 depicts the proposed lamellar structure suggested by the combined glycerol and d_{25}-SDS profiles (Figure 9) as well as possible hydrogen-bonding interactions between the surfactant headgroups and glycerol. The formation of organized surfactant nanostructures on the surface of the film is further supported by AFM, where the platelike structure most probably corresponds to a surface defect in the bilayer structure. The consistent height of this nanostructure, combined with its irregular (noncircular) shape, suggests that the feature is lamellar and sufficiently solid to be immobile on the timescale of the AFM scans (10s of minutes). It appears that these features are partial layers of d_{25}-SDS on the film surface, which could give rise to some variation in the *average* thickness in the adsorbed d_{25}-SDS-rich layer measured by NRA and NR. This variation (1−2 nm) is in fact too small to resolve with NRA. In the case of NR, the effect is slightly more complex, but to a good approximation, the NR data should correspond to superposition reflectivity profiles arising from different integer numbers of layers, as simulated in Figure 4.

Role of Plasticizer in the Size of the Surface Excess. There is a significant increase (up to ∼3 fold) in the value of z^*(SDS) upon the addition of the plasticizer glycerol to the films. This is evident from the concentration profiles displayed in Figures 2 and 3, in which d_{25}-SDS is the only deuterium-labeled component. It is important to understand if the increase in z^* arising from glycerol is a thermodynamic or kinetic effect because this would guide the efforts to control the surfactant-blooming phenomena and the subsequent surface properties of the film. From the presence of mixed SDS−glycerol surface layers, it seems that there is a synergistic effect in the adsorption

DOI: 10.1021/acs.langmuir.7b04046
Langmuir 2018, 34, 1410−1418

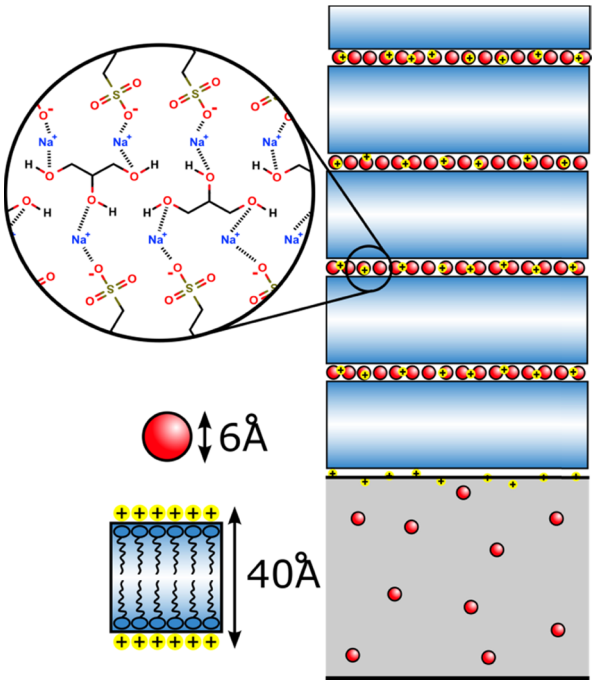

Figure 10. Schematic representation of the theorized multilamellae arrangement in a ternary plasticized film of SDS (blue), glycerol (red sphere), and PVA (gray). The diameter of glycerol and width of lamellae were obtained from Kiyosawa[34] and Coiro, respectively.

of SDS and glycerol on PVA surfaces. This is further supported by the surface tension analysis of mixed solutes (Figure 7), which indicates that the addition of glycerol, although it is minimally surface-active, enhances the surface tension reduction achieved by SDS at any given concentration. The spontaneous structuring of the surfactant and glycerol into smectic layers suggests a thermodynamically driven process; the system can minimize its free energy by (i) excluding the surfactant from the PVA-rich subphase and (ii) adopting an ordered lamellar structure with minimal perturbation to the PVA polymer chains. As suggested by the adhesion scans of the PVA film surfaces, the presence of strong and stable surfactant adsorbate layers does have a significant impact on surface properties. Although beyond the scope of this present work, we anticipate that other properties such as the wettability of the PVA film may also be significantly affected by blooming, such as we have found.

Although it does appear that the plasticizer does enable the formation of a thermodynamically stable wetting layer on the PVA surface, this does not exclude the possibility of a kinetic contribution. It remains a possibility that similar structures are thermodynamically favorable in the unplasticized films, but these become kinetically trapped before this can form as the drying film solidifies. This hypothesis is consistent with the observation of a depleted concentration in the near-surface region of unplasticized films (Figure 1), which was not found in the plasticized films (Figure 2).

CONCLUSIONS

Surface segregation of an anionic surfactant (SDS) in PVA leads to wetting layers of surfactant in spin-cast films. The presence of glycerol plasticizer in these films significantly increases the surface excess and enables the formation of smectic layers of alternating glycerol and surfactant on the PVA surface. In the case of plasticized films, nearly all of the surfactant migrates to the surface of (100 nm) thick films, whereas a significant proportion of the surfactant is retained in the PVA film when glycerol is absent. Variation of deuterium labeling enabled the isolation of composition versus depth profiles for SDS and glycerol in separate experiments. These composition profiles were found to be remarkably complementary and were consistent with the glycerol forming interstitial layers between the SDS lamellae. Our results are consistent with previous bulk studies[22] on SDS in aqueous environments, but we are unaware of any comparable study showing a similar assembly enabled by plasticizers on polymers.

Complementary surface tension measurements showed that although glycerol has almost no surface activity in pure water, it plays an important synergistic role in the adsorption of SDS, which underpins the formation of mixed surfactant/plasticizer layers on the surface of drying PVA films. Cloud point analysis over the composition range relevant to the drying films shows that phase separation occurs when the water content falls below 55% (w/w). The magnitude of the wetting layers formed, particularly in the plasticized films, indicates that the components remain mobile until the water content reaches significantly lower levels.

Controlling the formation and stability of surfactant blooms on polymer films has significant implications for their surface properties and applications. We find that a simple plasticizer, having no inherent surface activity of its own, can have a transformative effect on these properties.

ASSOCIATED CONTENT

Supporting Information

The Supporting Information is available free of charge on the ACS Publications website at DOI: 10.1021/acs.langmuir.7b04046.

Tabulated fit parameters for NR and IBA experiments; RBS analysis; fits to NR data in which lamellar structures are omitted; fitted NR profiles including roughness in lamellar structures; and AFM height and adhesion maps for additional control samples (PDF)

AUTHOR INFORMATION

Corresponding Author

*E-mail: r.l.thompson@dur.ac.uk, r.l.thompson@durham.ac.uk.

ORCID

Richard L. Thompson: 0000-0002-3207-1036

Notes

The authors declare no competing financial interest.

ACKNOWLEDGMENTS

We are grateful to EPSRC/Procter and Gamble (UK) and the Soft Matter and Functional Interfaces CDT (SOFI-CDT) for supporting this work via EP/L015536/1 and CASE award EP/L505419/1 and to STFC for provision of the neutron reflection facilities through beamtime allocation RB1510333 (https://doi.org/10.5286/isis.e.58452174).

REFERENCES

(1) Moukwa, M.; Youn, D.; Hassanali, M. Effects of degree of polymerization of water soluble polymers on concrete properties. *Cem. Concr. Res.* **1993**, *23*, 122−130.

DOI: 10.1021/acs.langmuir.7b04046
Langmuir 2018, 34, 1410−1418

(2) Termonia, Y.; Meakin, P.; Smith, P. Theoretical study of the influence of the molecular weight on the maximum tensile strength of polymer fibers. *Macromolecules* **1985**, *18*, 2246−2252.
(3) Mohsin, M.; Hossin, A.; Haik, Y. Thermal and mechanical properties of poly(vinyl alcohol) plasticized with glycerol. *J. Appl. Polym. Sci.* **2011**, *122*, 3102−3109.
(4) Gundabala, V. R.; Zimmerman, W. B.; Routh, A. F. A Model for Surfactant Distribution in Latex Coatings. *Langmuir* **2004**, *20*, 8721−8727.
(5) Gromer, A.; Thalmann, F.; Hébraud, P.; Holl, Y. Simulation of Vertical Surfactant Distributions in Drying Latex Films. *Langmuir* **2017**, *33*, 561−572.
(6) Briddick, A.; Li, P.; Hughes, A.; Courchay, F.; Martinez, A.; Thompson, R. L. Surfactant and Plasticizer Segregation in Thin Poly(vinyl alcohol) Films. *Langmuir* **2016**, *32*, 864−872.
(7) Hines, J. D.; Fragneto, G.; Thomas, R. K.; Garrett, P. R.; Rennie, G. K.; Rennie, A. R. Neutron Reflection from Mixtures of Sodium Dodecyl Sulfate and Dodecyl Betaine Adsorbed at the Hydrophobic Solid/Aqueous Interface. *J. Colloid Interface Sci.* **1997**, *189*, 259−267.
(8) Thompson, R. L. Surface and Interfacial Characterization: Ion Beam Analysis. In *Polymer Science: A Comprehensive Reference*; Moeller, M., Matyjaszwewski, K., Eds.; Elsevier BV: Amsterdam, 2012; Vol. 2, pp 661−681.
(9) Jeynes, C.; Colaux, J. L. Thin film depth profiling by ion beam analysis. *Analyst* **2016**, *141*, 5944.
(10) Composto, R. J.; Walters, R. M.; Genzer, J. Application of ion scattering techniques to characterize polymer surfaces and interfaces. *Mater. Sci. Rep.* **2002**, *38*, 107.
(11) Clough, A. S.; Collins, S. A.; Gauntlett, F. E.; Hodgson, M. R.; Jeynes, C.; Rihawy, M. S.; Todd, A. M.; Thompson, R. L. In situ water permeation measurement using an external He-3(2+) ion beam. *J. Membr. Sci.* **2006**, *285*, 137−143.
(12) Barradas, N. P.; Jeynes, C.; Webb, R. P. Simulated annealing analysis of Rutherford backscattering data. *Appl. Phys. Lett.* **1997**, *71*, 291−293.
(13) Jeynes, C.; Bailey, M. J.; Bright, N. J.; Christopher, M. E.; Grime, G. W.; Jones, B. N.; Palitsin, V. V.; Webb, R. P. "Total IBA"—Where are we? *Nucl. Instrum. Methods Phys. Res., Sect. B* **2012**, *271*, 107−118.
(14) Barradas, N. P.; Jeynes, C. Advanced physics and algorithms in the IBA DataFurnace. *Nucl. Instrum. Methods Phys. Res., Sect. B* **2008**, *266*, 1875−1879.
(15) Jeynes, C.; Barradas, N. P.; Szilágyi, E. Accurate Determination of Quantity of Material in Thin Films by Rutherford Backscattering Spectrometry. *Anal. Chem.* **2012**, *84*, 6061−6069.
(16) Penfold, J. Neutron reflectivity and soft condensed matter. *Curr. Opin. Colloid Interface Sci.* **2002**, *7*, 139−147.
(17) Welbourn, R. J. L.; Bartholomew, F.; Gutfreund, P.; Clarke, S. M. Neutron Reflectometry of an Anionic Surfactant at the Solid−Liquid Interface under Shear. *Langmuir* **2017**, *33*, 5982−5990.
(18) Harroun, T. A.; Fritzsche, H.; Watson, M. J.; Yager, K. G.; Tanchak, O. M.; Barrett, C. J.; Katsaras, J. Variable temperature, relative humidity (0%−100%), and liquid neutron reflectometry sample cell suitable for polymeric and biomimetic materials. *Rev. Sci. Instrum.* **2005**, *76*, 065101.
(19) Torikai, N.; Yamada, N. L.; Noro, A.; Harada, M.; Kawaguchi, D.; Takano, A.; Matsushita, Y. Neutron Reflectometry on Interfacial Structures of the Thin Films of Polymer and Lipid. *Polym. J* **2007**, *39*, 1238−1246.
(20) Mason, T. E.; Gaulin, B. D.; Garrett, J. D.; Tun, Z.; Buyers, W. J. L.; Isaacs, E. D. Neutron-scattering measurements of long-range antiferromagnetic order in URu2Si2. *Phys. Rev. Lett.* **1990**, *65*, 3189−3192.
(21) Huang, Q.; Qiu, Y.; Bao, W.; Green, M. A.; Lynn, J. W.; Gasparovic, Y. C.; Wu, T.; Wu, G.; Chen, X. H. Neutron-Diffraction Measurements of Magnetic Order and a Structural Transition in the Parent BaFe2As2 Compound of FeAs-Based High-Temperature Superconductors. *Phys. Rev. Lett.* **2008**, *101*, 257003.
(22) Coiro, V. M.; Manigrasso, M.; Mazza, F.; Pochetti, G. Structure of a triclinic phase of sodium dodecyl sulfate monohydrate. A comparison with other sodium dodecyl sulfate crystal phases. *Acta Crystallogr., Sect. C: Struct. Chem.* **1987**, *43*, 850−854.
(23) Hernáinz, F.; Caro, A. Variation of surface tension in aqueous solutions of sodium dodecyl sulfate in the flotation bath. *Colloids Surf., A* **2002**, *196*, 19−24.
(24) Mysels, K. J. Surface tension of solutions of pure sodium dodecyl sulfate. *Langmuir* **1986**, *2*, 423−428.
(25) Polmanteer, K. E. Current perspectives on silicone rubber technology. *Rubber Chem. Technol.* **1981**, *54*, 1051−1080.
(26) Wu, S. Estimation of the critical surface tension for polymers from molecular constitution by a modified Hildebrand-Scott equation. *J. Phys. Chem.* **1968**, *72*, 3332.
(27) Lee, L.-H. Relationships between surface wettability and glass temperatures of high polymers. *J. Appl. Polym. Sci.* **1968**, *12*, 719.
(28) Hoftyzer, P. J.; van Krevelen, D. W. The newtonian shear viscosity of concentrated polymer solutions. *Angew. Makromol. Chem.* **1976**, *56*, 1−14.
(29) van Oss, C. J.; Chaudhury, M. K.; Good, R. J. Monopolar surfaces. *Adv. Colloid Interface Sci.* **1987**, *28*, 35−64.
(30) Takamura, K.; Fischer, H.; Morrow, N. R. Physical properties of aqueous glycerol solutions. *J. Pet. Sci. Eng.* **2012**, *98*−*99*, 50−60.
(31) Frisch, H. L.; Al-Madfai, S. Surface Tension of Synthetic High Polymer Solutions1. *J. Am. Chem. Soc.* **1958**, *80*, 3561−3565.
(32) Sammalkorpi, M.; Karttunen, M.; Haataja, M. Ionic Surfactant Aggregates in Saline Solutions: Sodium Dodecyl Sulfate (SDS) in the Presence of Excess Sodium Chloride (NaCl) or Calcium Chloride (CaCl2). *J. Phys. Chem. B* **2009**, *113*, 5863−5870.
(33) Bagdassarian, C. K.; Roux, D.; Ben-Shaul, A.; Gelbart, W. M. Curvature defects in lamellar phases of amphiphile-water systems. *J. Chem. Phys.* **1991**, *94*, 3030−3041.
(34) Kiyosawa, K. Volumetric properties of polyols (ethylene glycol, glycerol, meso-erythritol, xylitol and mannitol) in relation to their membrane permeability: Group additivity and estimation of the maximum radius of their molecules. *Biochim. Biophys. Acta, Biomembr.* **1991**, *1064*, 251−255.

DOI: 10.1021/acs.langmuir.7b04046
Langmuir 2018, 34, 1410−1418